Results in Engineering 26 (2025) 104914

Contents lists available at ScienceDirect

Results in Engineering

journal homepage: www.sciencedirect.com/journal/results-in-engineering

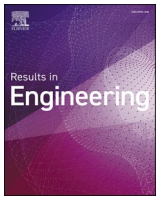

Thermal management in a phase change material-based microchannel heat sink manifold system for cooling electronic boards

Ali B.M. Ali [a], Sabah F.H. Alhamdi [b], Mohammad M.S. Al-Azawii [b], Narinderjit Singh Sawaran Singh [c], Mohammad Ali Fazilati [d,*], Soheil Salahshour [e,f,g], S. Ali Eftekhari [d,*]

[a] Air Conditioning Engineering Department, College of Engineering, University of Warith Al-Anbiyaa, Karbala, Iraq
[b] Department of Mechanical Engineering, University of Misan, Amarah, Misan, 62001, Iraq
[c] Faculty of Data Science and Information Technology, INTI International University, Persiaran Perdana BBN, Putra Nilai, Nilai, 71800, Malaysia
[d] Department of Mechanical Engineering, Khomeinishahr branch, Islamic Azad University, Khomeinishahr, Iran
[e] Faculty of Engineering and Natural Sciences, Istanbul Okan University, Istanbul, Turkey
[f] Faculty of Engineering and Natural Sciences, Bahcesehir University, Istanbul, Turkey
[g] Research Center of Applied Mathematics, Khazar University, Baku, Azerbaijan

ARTICLE INFO

Keywords:
Microchannel manifold
Thermal management
PCM board
Computational fluid dynamics (CFD)

ABSTRACT

The growth of technology and the development of electronic devices made the need for efficient thermal management. By the ability of latent thermal energy storage, the application of phase change materials (PCMs) for cooling electronic boards has been investigated. The heat sink is an air-cooled micro heat sink cooling system (MHCS) with the possibility of embedding the PCM board. A type of metal-based paraffin is the PCM and free and forced modes of convective cooling studied numerically. Five input heat fluxes and three Reynolds (*Re*) numbers were investigated and the system performance was analyzed. The results show the significant influence of PCM on the control of the EC temperature; the reduction of heat sink temperature by 72 % and 78 % in natural and forced convection modes respectively, are the results of employing PCM in MHCS. It was shown that the best result of PCM employment in forced convection mode is at the lowest *Re* number. Furthermore, the *Re* number increase has the best effect on cooling efficiency at the highest heat flux. The results of this study could help in justifying the application of PCM from technical and economic viewpoints.

1. Introduction

The outstanding progress in electronic equipment and the ever-increasing need for miniaturization lead to the problem of overheating, reduction of performance, efficiency, and lifetime [1,2]. The high working temperature is the reason for most failures in electronic components [3] which approves the significance of thermal management in the systems. Different techniques could be implemented for chip cooling including air cooling, embedded cooling, immersion cooling, electrocaloric cooling, spray cooling, jet cooling, heat pipe, thermoelectric cooling, and microchannel cooling [4]. In most cooling techniques, the heat dissipation of heat sink in micro size (*MCHS*) or macro size is done through the cooling fluid flow. The cooling fluid could be in a liquid or gas state and usually water and air are used. The literature review observed that heat transfer enhancement usually takes place at the penalty cost of pressure drop and other flow complications [5]. Due to its inherent higher surface area-to-volume ratio, using the micro-channel heat sink (*MCHS*) has emerged as an innovative and efficient solution for solving the heating issues in electronic components. Prabhakar Bhandari et al. [5] comprehensively reviewed the literature on *MCHS*s and the prominent design modifications for their heat transfer improvement. Tuckerman and Pease [6] were the first ones who examine the rates of flow and heat exchange at the microscale. They

Abbreviations: 3D, 3 dimensional; *AR*, aspect ratio; *cp*, specific heat (kJ/kg.K); *Cu*, copper; *D*, hydraulic diameter; *EC*, electric circuit; *FVM*, finite volume method; *g*, ground gravity acceleration (m/s^2); *h*, specific enthalpy (kJ/kg); *H*, enthalpy (kJ); *k*, conductivity (W/m.K); *LHS*, latent heat storage; *MCHS*, microchannel heat sink; *NF*, nanofluid; *NP*, nanoparticle; *Nu*, Nusselt number; *PCM*, phase change material; *Re*, Reynolds number; *S*, source term (kPa/m); *VOF*, volume of fluid; *p*, pressure (kPa); $\ddot{q}$, heat flux (W/m^2); *T*, temperature (°C); *u*, velocity (m/s); *v*, perpendicular velocity (m/s); *x*, length (m).

* Corresponding authors.
E-mail addresses: mafazilati@iau.ac.ir (M.A. Fazilati), s.A.Eftekhari@iaukhsh.ac.ir (S.A. Eftekhari).

https://doi.org/10.1016/j.rineng.2025.104914
Received 4 July 2024; Received in revised form 28 February 2025; Accepted 11 April 2025
Available online 11 April 2025

Nomenclature

Greek symbols

Δ	difference
ν	dynamic velocity (m^2/s)
ρ	density (kg/m^3)

Subscripts

a	air
b	bulk
m	melting
sf	solid to fluid
w	wall

experimentally showed that a rectangular microchannel has a noticeable heat dissipation rate and could maintain the temperature near the ambient temperature. In this way, the effects of geometry modification [7,8], working fluids and flow configurations [9,10] have been studied on the thermal performance of the *MCHS* [11,12]. The heat transfer effects of aspect ratio (*AR*) and hydraulic diameter in a rectangular *MCHS* were studied by Amirah M. Sahar et al. [13]. Their findings showed that by increasing the *AR* to 2 the friction factor decreased a bit and then increased by increasing it. Through a *3D* numerical simulation, Moradikazerouni et al. [14] studied the airflow in an *MCHS* with different entrance channel geometries. The effect of air temperature and velocity on the pressure drop and *Nu* number was investigated. They found that between the investigated geometries, for the triangular channel the thermal performance is the best but considering the construction issues, the circular channel is recommended. Navin Raja Kuppusamy et al. [15,16] conducted numerical work on *MCHS* using the

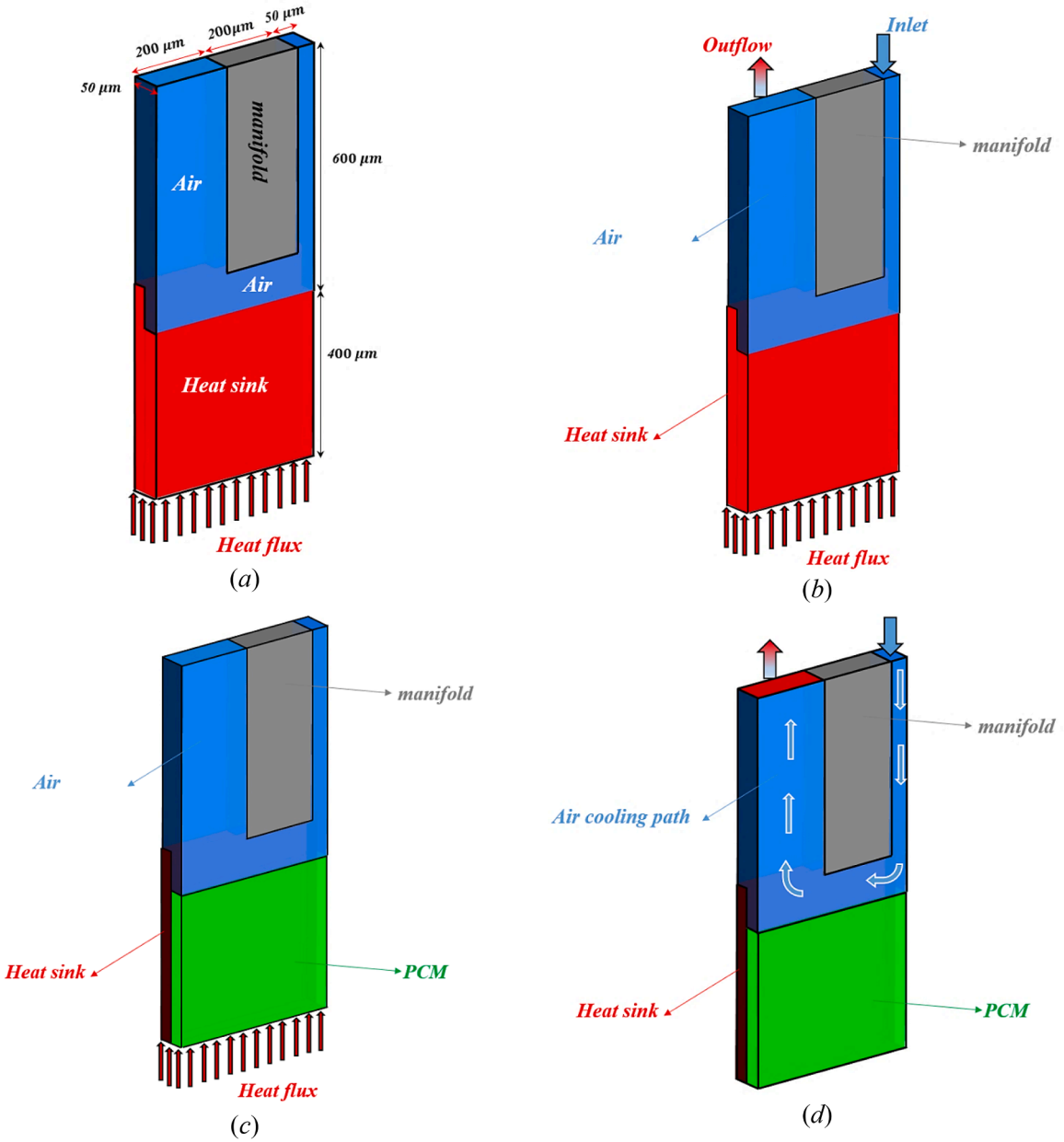

Fig. 1. The schematic of the studied problem in four different conditions and dimensions, *a*) natural convection without *PCM, b*) forced convection without *PCM, c*) natural convection with the embedded *PCM, d*) forced convection with the embedded *PCM*.

Table 1
PCM type and its thermophysical properties.

PCM type	T_m (°C)	$h_{sf}\left(\frac{kJ}{kg}\right)$	$\rho\left(\frac{kg}{m^3}\right)$	$C_p\left(\frac{kJ}{kg.K}\right)$	$k\left(\frac{W}{m.K}\right)$
49Bi-21In-18Pb-12Sn	58	202	9079	3230	33.2

Table 2
The investigated heat flux and *Re* number.

Heat flux (kW/m^2)	*Re* number
150, 170, 180, 190, 210	20, 40, 60

NF as the working fluid. They found the improvement in *MCHS* with triangular and trapezoidal shaped grooves with better results for trapezoidal compared to rectangular grooves. The studies on *MCHS* show the improving effect of using *NF* on thermal behavior [17–19]. Through numerical work, Chein and Huang [20] investigated the performance of a rectangular *MCHS*; the *NF* of water/*Cu* was chosen as the working fluid and the effect of nanoparticle (*NP*) concentration was studied. The results show the enhancement in performance of *MCHS* compared to the case of using water as a coolant. In most research around the *MCHS,* the focus is on heat transfer improvement by increasing the heat transfer surface and enhancing the working fluid characteristics and the ways to mitigate pressure loss increment resulted by the increased heat transfer area.

Besides these methods, phase change materials (*PCM*) could also be used in *MCHS*. By their benefits, *PCM*s have found large applications in thermal management systems [17,21–24]. The *PCM*s have been used as a latent energy storage medium in different systems including heat exchangers, electric circuits, structures, etc. [25,26]. *PCM*s can absorb or release large amounts of energy at a fixed temperature. The heat transfer studies of heat sinks equipped with *PCM*s showed enhancements in the thermal characteristics of these systems [27]. The phase change heat storage techniques enhance the replication of electronic devices and increase the capacitance of the cooling apparatus, delaying temperature augmentation and eventually having an improving effect on thermal management [28]. The application of *PCM*s with the combination of other thermal management techniques could result in efficient heat collection, transmission and dissipation in *MCHS* systems [29,30]. With the added advantage of increased effective surface area, the *PCM*-microchannel combination system benefited from the isothermal situation during the phase change time. This feature besides the large heat of fusion falls down the maximum temperatures and prevents the hot spots during the melting time. By the integration of *PCM*s into the heat sinks of *EC*s, the thermal inertia of the cooling system would be enhanced. *PCM*s are capable of absorbing and releasing high amounts of energy during melting and solidification processes. This feature regulates the temperature effectively and prevents the *EC*s from overheating [31]. To avoid the abrupt failure of electric circuits (*EC*s), it is important to keep their working temperature below 80–90 °C [32]. The proper application and lifetime of *EC*s are in inverse relation to their temperature and it needs the proper thermal management [33]. Within the turn-off periods of the *EC, PCM* undergoes the liquid-to-solid phase change and releases heat. In summary, thermal control devices should be employed in place of peak power periods [34]. Despite the large applications of PCMs in thermal management systems [34], the application of *PCM* in *MCHS* for transient thermal management working in high-power heat transfer requires specific *PCM* types capable of faster rates of heat absorption. These *PCM*s are materials with high thermal conductivity, specifically metallic *PCM*s. Metallic *PCM*s could absorb heat up to 200 % faster than other classes of *PCM*s [35], and at fluctuating rate appropriate for *EC* cooling performance. W Yan et al. [36] studied the *MCHS* by embedding the *PCM* in the ceiling and the *NF* of water-Al_2O_3 as the working fluid. The application of 10 % *NF* reduced the thermal resistance of the heat sink by 10.88 %. Ho et al. [2] implemented the water-nano-encapsulated *PCM* in a microchannel. Their findings show the improvement of the heat transfer index by >40 %. Motahar and Jahangiri [21] worked on the *PCM* heat sink through the experimental and neural network analysis approaches. They reported a reduction in working temperature during the heating process as a result of implementing the *PCM*. Wang et al. [37] reported the transient cooling performance of a novel spiral heat sink device. The heatsink of two eccentric spirals with the first spiral filled partially with paraffin wax and the other with air flow was examined. The input heat transfer rates of 2.9 W to 3.7 W were tested. The results show 44.91 % performance improvement of system by the *PCM* application. In a numerical work, Hasan and Tbena [38] considered the application of paraffin wax, Eicosane, *P116* and *RT41* as the *PCM* in a microchannel and reported the enhancement in the cooling performance. Chen et al. [39] studied the thermal/flow characteristics of a (*MCHS*) with the embedded *PCM*. Through the numerical *3D* finite volume method a more uniform temperature and cooling efficiency was found; also, they obtained the optimum geometric dimensions. To deal with the fluctuating heat generated from the electronic components, Naga Ramesh Korasikha et al. [40] modeled *PCM* inserts embedded *MCHS*. They modeled the performance of *MCHS* in two cases of with and without using *PCM* by *ANSYS Fluent* software. Their findings show 12 % improvement in thermal performance factor and 7.3 % reduction of thermal resistance for *PCM* based system.

Based on the authors' knowledge, studies on the transient behavior of *PCM*-embedded *MCHS*s are rare and require further development. Here the dynamic and steady state behavior of a *PCM*-embedded *MCHS* system is studied. The dynamic and steady-state performance of the system was investigated in both natural and forced convection cooling. Heat sink temperature and *Nu* number as the heat transfer characteristics and *PCM* temperature and liquid fraction as the heat storage evaluation indexes examined. After the problem description, the modeling procedure and the governing equations, in the next sections, the evaluation indexes are presented vs the time by which the system performance is discussed.

2. The statement of the problem and governing relations

The studied system with the main dimension is schematically depicted in four different modes as specified in Fig. 1. The inlet heat flux is applied at the bottom and the microchannel could be used in both free and forced convection heat transfer modes. The system is a heat sink whose performance is studied in four different modes as specified in Fig. 1 by *a* to *d*; the inlet heat flux is applied at the bottom and the microchannel could be used in both free and forced convection heat transfer modes. For investigating the effect of using latent heat storage (*LHS*) on thermal performance, the module also can have the *PCM* board at the bottom. As can be seen, the manifold is located between the inlet and outlet air channels.

The heat sink thermal and fluid flow characteristics are investigated by exploring the mean temperature of the heat sink and the *PCM* liquid fraction and temperature at different inlet heat fluxes; also, to reveal the physics of the problem, the temperature counters of airflow and streamlines are visualized. The properties of the used *PCM* are shown in Table 1. Long-term performance and stability of employed PCM in repeated cooling cycles has been proved experimentally [41].

The fluid type is air throughout the study; the fluid behavior is judged as Newtonian and the finite volume method (*FVM*) is used for thermo flow modeling. The simulations are organized in two working modes of natural and forced convection and under the fixed input heat flux. The values of the *Re* number in forced convection mode and the inlet heat flux are listed in Table 2. The velocity of air is determined by employing the equation of *Re* number (Eq. (1))

$$\mathrm{Re} = \frac{u_{ave} D_h}{\nu} \tag{1}$$

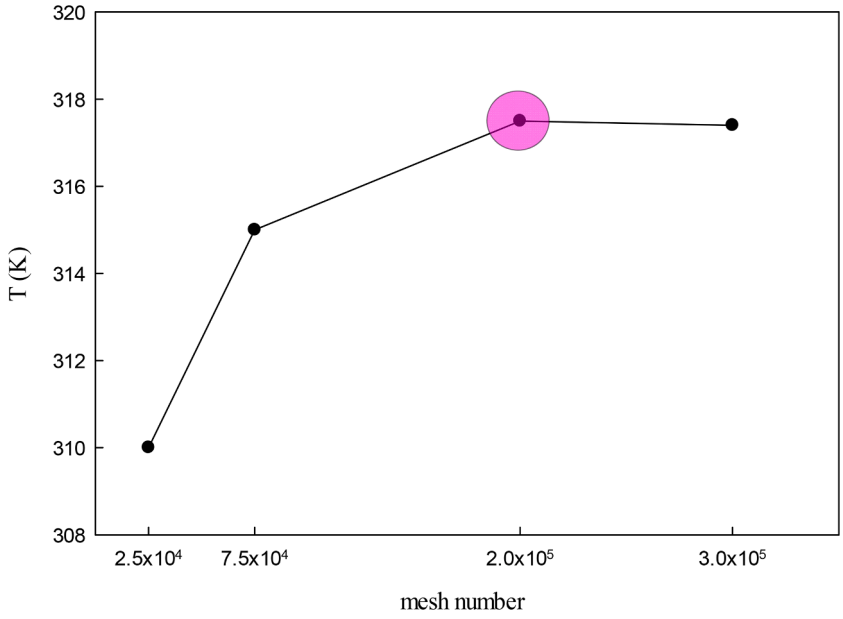

Fig. 2. The average air temperature for different mesh numbers.

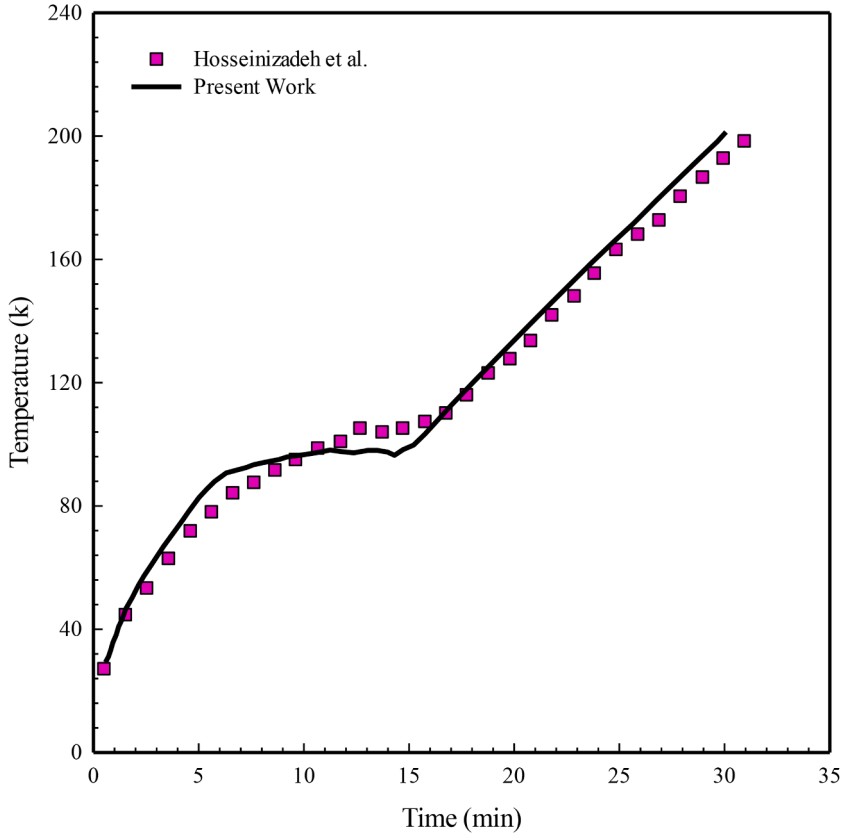

Fig. 3. The variation of heat sink temperature obtained by the previous experimental [46] and present work.

For the heat transfer analysis, the *Nu* number according to Eq. (2), has been used.

$$Nu_x = \frac{h_x D_h}{k} \tag{2}$$

The parameter h_x in Eq. (2) is the coefficient of heat transfer whose value is calculated by Eq. (3). In Eq. (3) T_b is the fluid flow mean temperature and is calculated by Eq. (4). Also the average Nu number is according to Eq. (5).

$$h_x = \frac{q''}{T_w - T_b} \tag{3}$$

$$T_b = \frac{\sum(\dot{m}T)}{\sum \dot{m}} \tag{4}$$

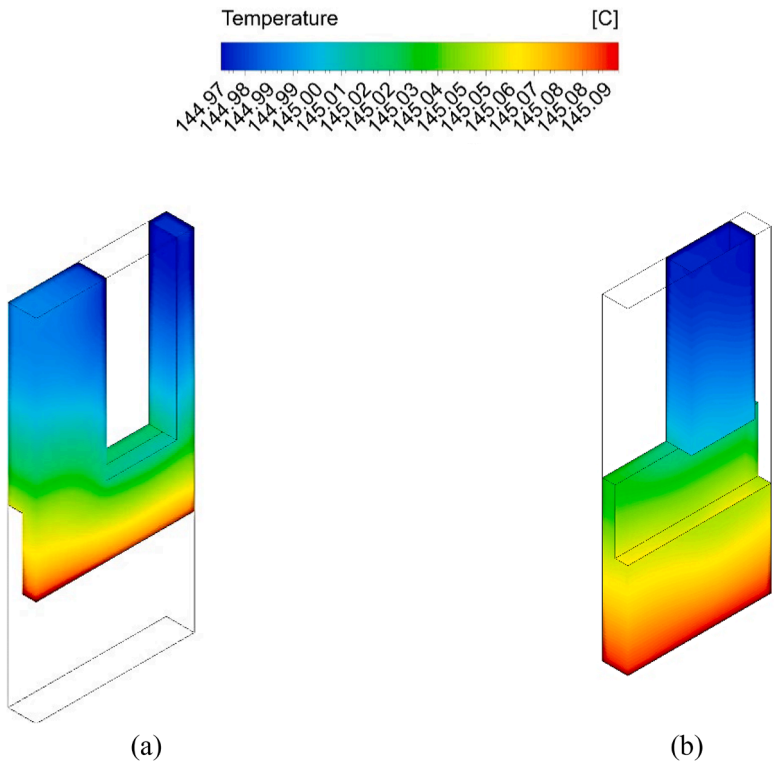

Fig. 4. Temperature contours in a) air side and b) solid side of heat sink.

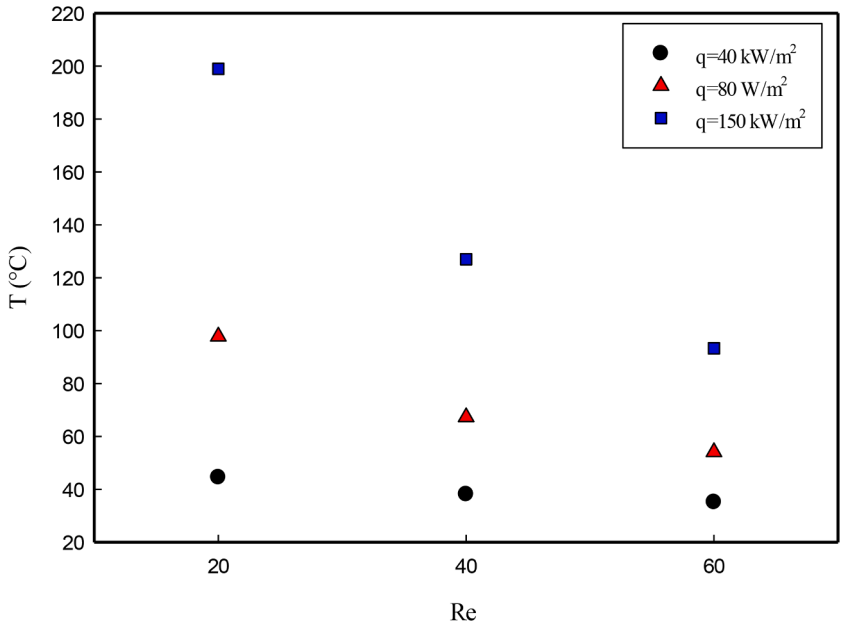

Fig. 5. The average temperature of heat sink vs the *Re* number for different input heat fluxes.

$$Nu_{ave} = \frac{q'' D_h}{k_f (T_w - T_b)} \tag{5}$$

Governing equations of the air-side flow consist of the conservation of mass, momentum, and energy equations. In obtaining these equations the following assumptions were made;

- the airflow behaves like a Newtonian fluid;
- incompressible fluid flow;
- the natural convection of heat transfer in the liquid *PCM*;
- the insulated heat sink outer walls and the heat transfer only between the airflow (*HTF*) and *PCM*;

Considering the pre-mentioned assumptions, the equations mass, momentum, and energy conservation for the air-side flow could be written as Eqs. (6), (7) and (8) respectively [23].

$$\frac{\partial}{\partial x_i}(u_i) = 0 \tag{6}$$

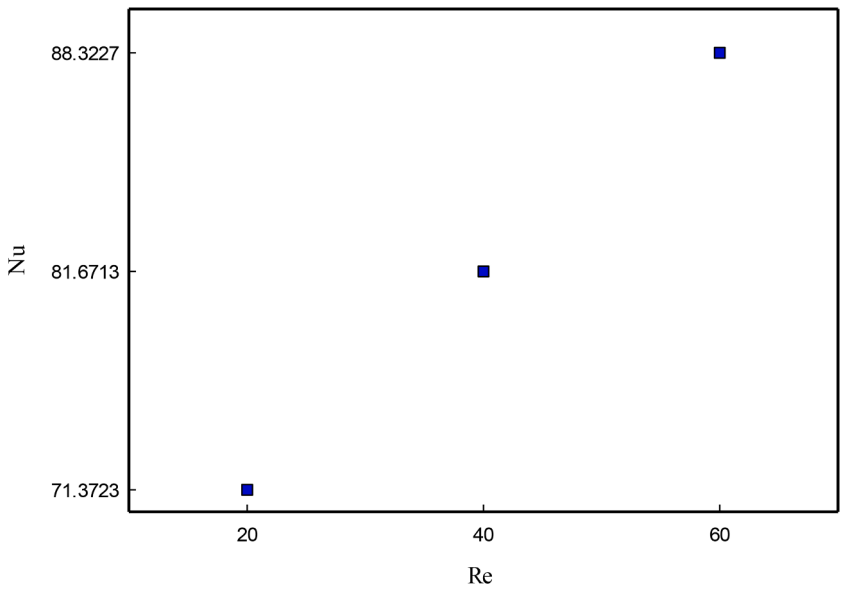

Fig. 6. The *Nu* number against the *Re* number at a heat flux of 150kW/m^2.

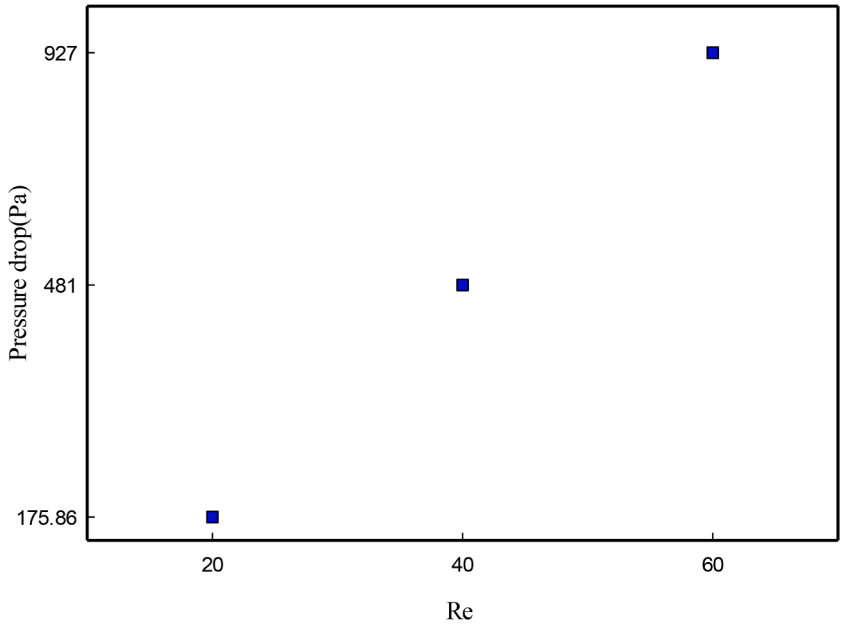

Fig. 7. The variation of pressure drop vs the *Re* number at a heat flux of 150 kW/m^2.

$$u_j\frac{\partial\overline{u_i}}{\partial x_j}+\frac{1}{\rho}\frac{\partial\overline{P}}{\partial x}=\nu\left(\frac{\partial^2\overline{u}_i}{\partial x_j\partial x_j}\right)-\frac{\partial\left(\overline{u_i'v_i'}\right)}{\partial x_j} \tag{7}$$

$$\rho c_p\left(u_i\frac{\partial T}{\partial x_i}\right)=k\left(\frac{\partial^2 T}{\partial x_{i,i}}\right) \tag{8}$$

For the *PCM* side, the conservation of mass and momentum equations could be expressed as Eqs. (7) and (9), respectively [24].

$$\frac{\partial(\rho_n u_i)}{\partial t}+\frac{\partial}{\partial x_j}\left(\rho_n u_i u_j\right)=\frac{\partial \mathrm{P}}{\partial x_i}+\frac{\partial}{\partial x_j}\left[\mu_n\left(\frac{\partial u_i}{\partial x_j}+\frac{\partial u_j}{\partial x_i}-\frac{2}{3}\delta_{ij}\frac{\partial u_i}{\partial x_i}\right)\right]+\rho_n g_i+S \tag{9}$$

$$S=\frac{(1-\beta)^2}{\beta^3+\varepsilon}A_{mush}\left(\overrightarrow{v}-\overrightarrow{v_p}\right) \tag{10}$$

In Eq. (9), u represents velocity components, P denotes the pressure, ρ refers to density, g is the gravitate acceleration and S is the momentum source; also in Eq. (10), v and β are the solid velocity in melted *PCM* and the liquid fraction, respectively and A_{mush} and ε are both constant values which the latter is set to prevent the division to zero. The enthalpy porosity method is chosen for simulating the thermal behavior of *PCM*. In the enthalpy porosity method, instead of examining the melting surface, the liquid fraction is observed. The liquid fraction denotes the part of the calculation cell in a liquid state. The solving process includes the liquid fraction determination specified using the equation of enthalpy balance. The thermal energy stored in *PCM* is according to Eq. (11). In Eq. (11), the symbol H denotes the *PCM* enthalpy which is the summation of the latent heat (ΔH) and sensible heat (h);

$$H=h+\Delta H \tag{11}$$

By these definitions, the *PCM* side energy equation is expressed

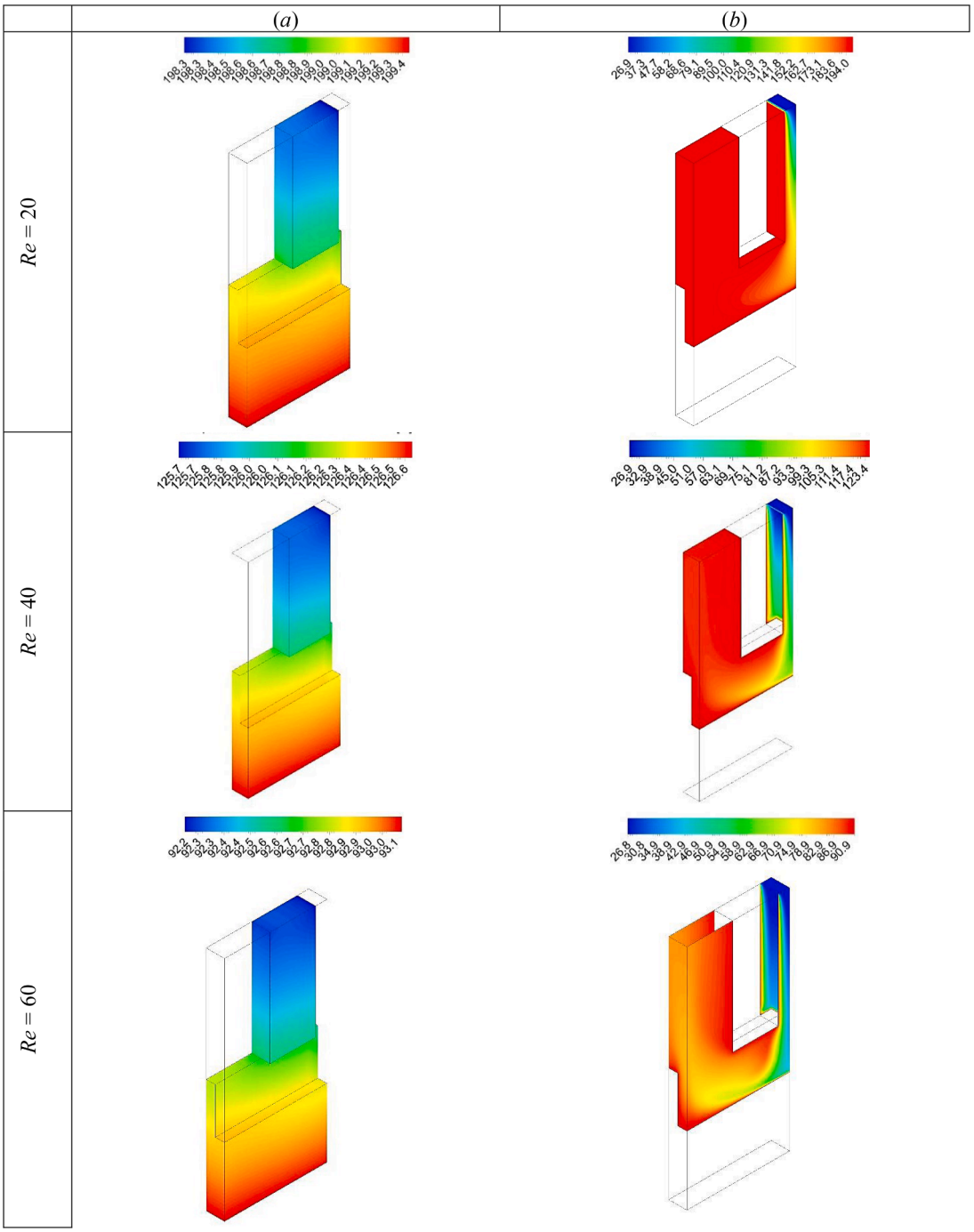

Fig. 8. Temperature contours for different *Re* numbers and heat flux of 150kW/m^2 in *a*) solid side and *b*) airside.

below [23];

$$\frac{\partial H}{\partial t} + \vec{\nabla}.(\overrightarrow{V}h) = \vec{\nabla}.\left(\frac{k}{\rho}\vec{\nabla}h\right) \tag{12}$$

Eq. (12), the sensible enthalpy is determined according to Eq. (13);

$$h = h_{ref} + \int_{T_{ref}}^{T} C_P \, dT \tag{13}$$

In Eq. (13), h_{ref} denotes the enthalpy at reference point, T_{ref} stands for temperature of reference, and C_P refers to specific heat. The parameter ΔH in Eq. (12) is determined by Eq. (14) in which L and α is the latent heat of the *PCM* and its liquid fraction, respectively. The liquid fraction of *PCM* (α) is determined using Eq. (15);

$$\Delta H = \alpha L \tag{14}$$

$$\alpha = \begin{cases} 0, & T < T_{solidus} \\ \dfrac{T - T_{solidus}}{T_{liquidus} - T_{solidus}}, & T_{Solidus} < T < T_{Liquidus} \\ 1, & T > T_{liquidus} \end{cases} \tag{15}$$

In Eq. (15) when the *PCM* temperature falls in a second interval, i.e. $T_{Solidus} < T < T_{Liquidus}$ both liquid and solid phases are existed and take place during the phase change. While the processes of solidification and melting, the energy equation presented as Eq. (16) [42]:

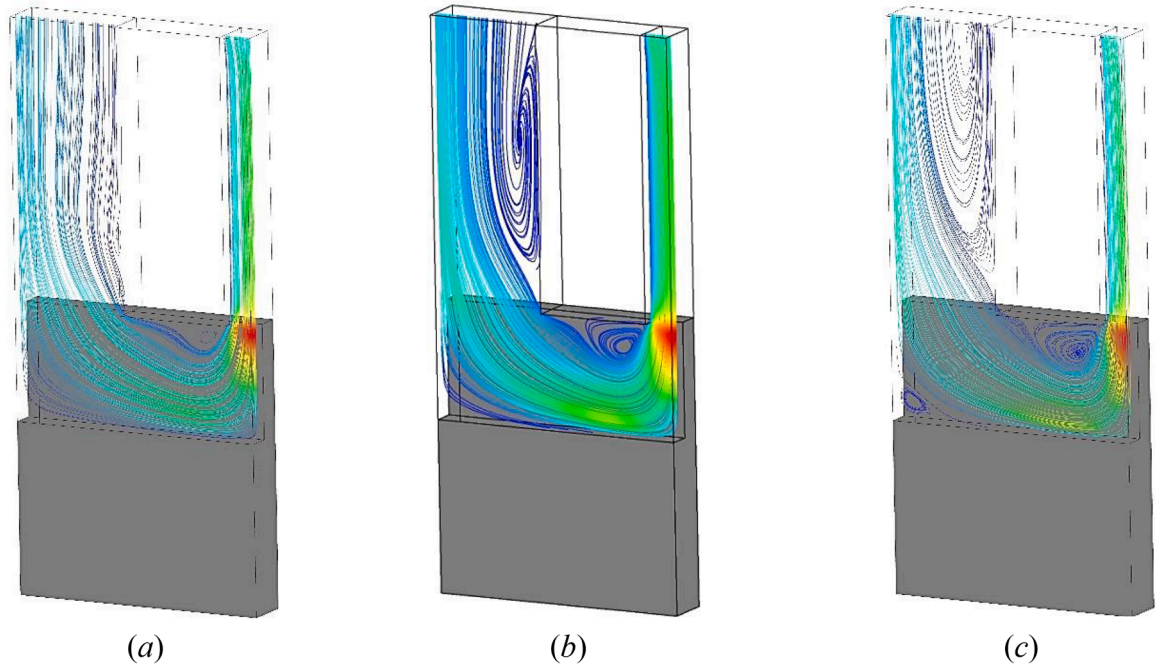

Fig. 9. The streamlines of air flow for different *Re* numbers of *a*) 20, *b*) 40 and *c*) 60.

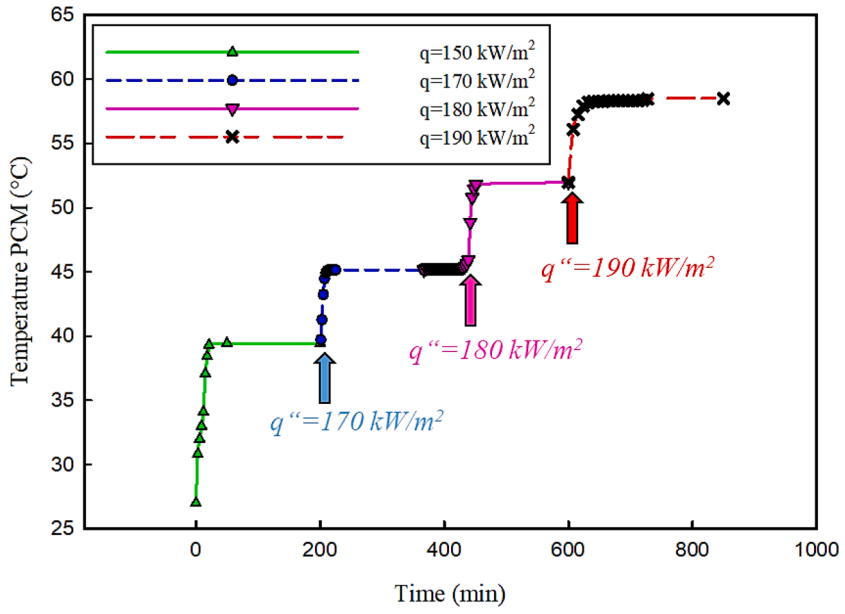

Fig. 10. The time variation of *PCM* temperature during the heat absorption in free convection working mode.

$$\frac{\partial(\rho H)}{\partial t}+\vec{\nabla}.(\rho\vec{v}H)=\vec{\nabla}.(k\vec{\nabla}T)+S \tag{16}$$

In Eq. (16), $\vec{v}$ denotes the velocity of fluid and S refers to the source of thermal energy. Within the method of enthalpy-porosity, the porous area is the region where the melting process happens. The porosity parameter is defined as the *PCM* liquid fraction in the cell. For a completely solid area, the value of porosity is equal to zero, and the velocity would be zero. For the *PCM* side the momentum equation is according to Eq. (17) [23];

$$\frac{\partial(\rho_n u_i)}{\partial t}+\frac{\partial}{\partial x_j}\left(\rho_n u_i u_j\right)=\frac{\partial \mathrm{P}}{\partial x_i}+\frac{\partial}{\partial x_j}\left[\mu_n\left(\frac{\partial u_i}{\partial x_j}+\frac{\partial u_j}{\partial x_i}-\frac{2}{3}\delta_{ij}\frac{\partial u_i}{\partial x_i}\right)\right]+\rho_n g_i+S \tag{17}$$

In the momentum equation, the parameter S reflects the damping source about Darcy's law which shows the phase change impact on convection and is presented by Eq. (18) [43]:

$$S=\frac{(1-\beta)^2}{\beta^3+\varepsilon}A_{mush}\left(\vec{v}-\vec{v_p}\right) \tag{18}$$

In Eq. (19), β is the liquid phase volume fraction, ε is 0.001 for the prevention of dividing to zero, and $\vec{v_p}$ is solid velocity outside the domain; moreover A_{mush} is the factor of mushy zone and is considered as 10^6 [44]. For the present system composed of *PCM* and air, the *VOF* model is employed. In this model, the value of α_n, wiz the fraction filled in the cell, would be as below;

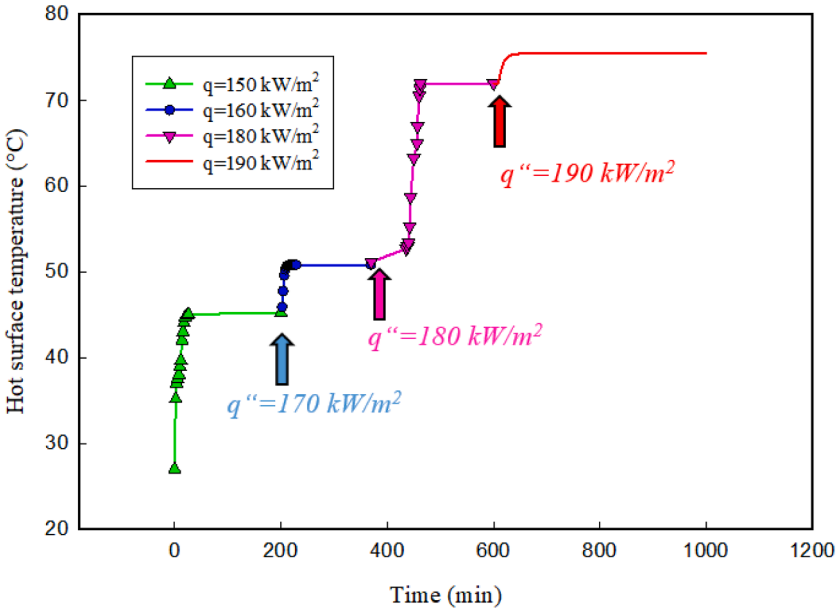

Fig. 11. The variation of *PCM* embedded heat sink temperature vs time during the heat absorption in natural convection mode.

- $\alpha_n = 0$, the nth cell is out of the fluid;
- $\alpha_n = 1$, is full of the fluid;
- $0 < \alpha_n < 1$, the nth cell is partly filled with the fluid.

In this way, the mass conservation equation would be according to Eq. (19);

$$\frac{\partial \alpha_n}{\partial t} + u_i \frac{\partial \alpha_n}{\partial x_i} = 0 \tag{19}$$

3. Numerical procedure

The governing equations with the associated boundary conditions were solved by employing the finite volume method. Discretization was done using the central differencing and *QUICK* schemes. The algorithm of *SIMPLE* is used to couple the velocity and pressure fields [45]. The convergence criterion of 10^{-6} was taken for all the engaged governing equations. The boundary conditions over the boundaries of the system are as follows; the inlet velocity for the inlet airflow, the pressure outlet for the outflow, no-slip condition for the walls, fixed heat flux for the bottom walls and thermal insulation for other walls.

To ascertain the independency and accuracy of the results from the selected mesh, the average air temperature was determined and depicted for different systems with different mesh numbers (Fig. 2). The figure shows that each time the grid mesh size reduction the value of T_a got close to its previous value until at a mesh number of 200,000, it nearly became fixed (changes <3 %). Hence, 200,000 was chosen as the cell number for the domain.

To verify the correctness of the numerical procedure, the simulation results were judged against the work of Hosseinzadeh et al. [46]. In their work, the behavior of a *PCM* heat sink was investigated both numerically and experimentally. The heat sink was finned type and the heat flux was exerted from beneath it. Also, they compared the thermal management performance of heat sinks in two cases with and without using *PCM*. They investigated the effects of power level, fin number, height and thickness. Fig. 3 compares the heat sink temperature obtained by the present numerical study and the previous work; it could be seen that the present numerical study is in good agreement with the previous experimental work within a 5 % mismatch; since in comparison with experimental works a difference of 15 % is acceptable, this simulation method would be approved [47].

4. Results and discussion

The system was meshed using the software package of *ANSYS* 19 and the equations were solved with *ANSYS FLUENT* software. The system performance was studied in two different modes with and without a *PCM* board. The results of simulation for different study cases (with and without *PCM* and natural and forced convection modes) were demonstrated by different evaluation indexes including convection heat transfer coefficient and *Nu* number, heat sink temperature, *PCM* liquid fraction and pressure drop and pumping power in forced convection mode; moreover, temperature contours and streamlines was presented to visualize thermal and flow physics of the system.

4.1. Heat sink without the PCM

4.1.1. Natural convection mode

The heat flux is first exerted on the solid side and eventually to the air. The still air above the solid side is heated and the resulting temperature gradient causes the heat transfer. The temperature contours in both solid (heat sink and manifold) and airside are shown in Fig. 4. The input heat flux is 40kW/m^2 and as can be seen a uniform temperature distribution is generated; in this case the heat sink mean temperature is 145 °C. By the higher-than-allowable temperature of the heat sink, the mode of free convection is not able for the successful release of heat and forced convection should be employed.

4.1.2. Forced convection mode

The mean temperature of the heat sink vs the *Re* number is depicted in Fig. 5. Firstly, it is shown that by switching the heat convection mode from natural to force, the mean temperature reduces significantly; the mean temperature at a heat flux of 40kW/m^2 is 44, 38 and 35 °C at *Re* numbers of 20, 40 and 60 which was 145 °C in natural convection mode; the corresponding values for heat fluxes of 80 and 150kW/m^2 are 100, 65, 55 °C and 200, 125 and 95 °C for *Re* numbers of 20, 40 and 60, respectively. The overall trend of temperature change against the *Re* number is decreasing and is the result of a higher heat transfer coefficient at higher *Re* numbers; by growing the *Re* number from 20 to 60, the mean temperature is reduced by 50 %, 40 % and 11 % at heat fluxes of 150, 80 and 40kW/m^2, respectively. This, on the other hand, shows the higher effect of *Re* number increase on cooling efficiency at higher heat fluxes which results in more temperature decrement and is not the case

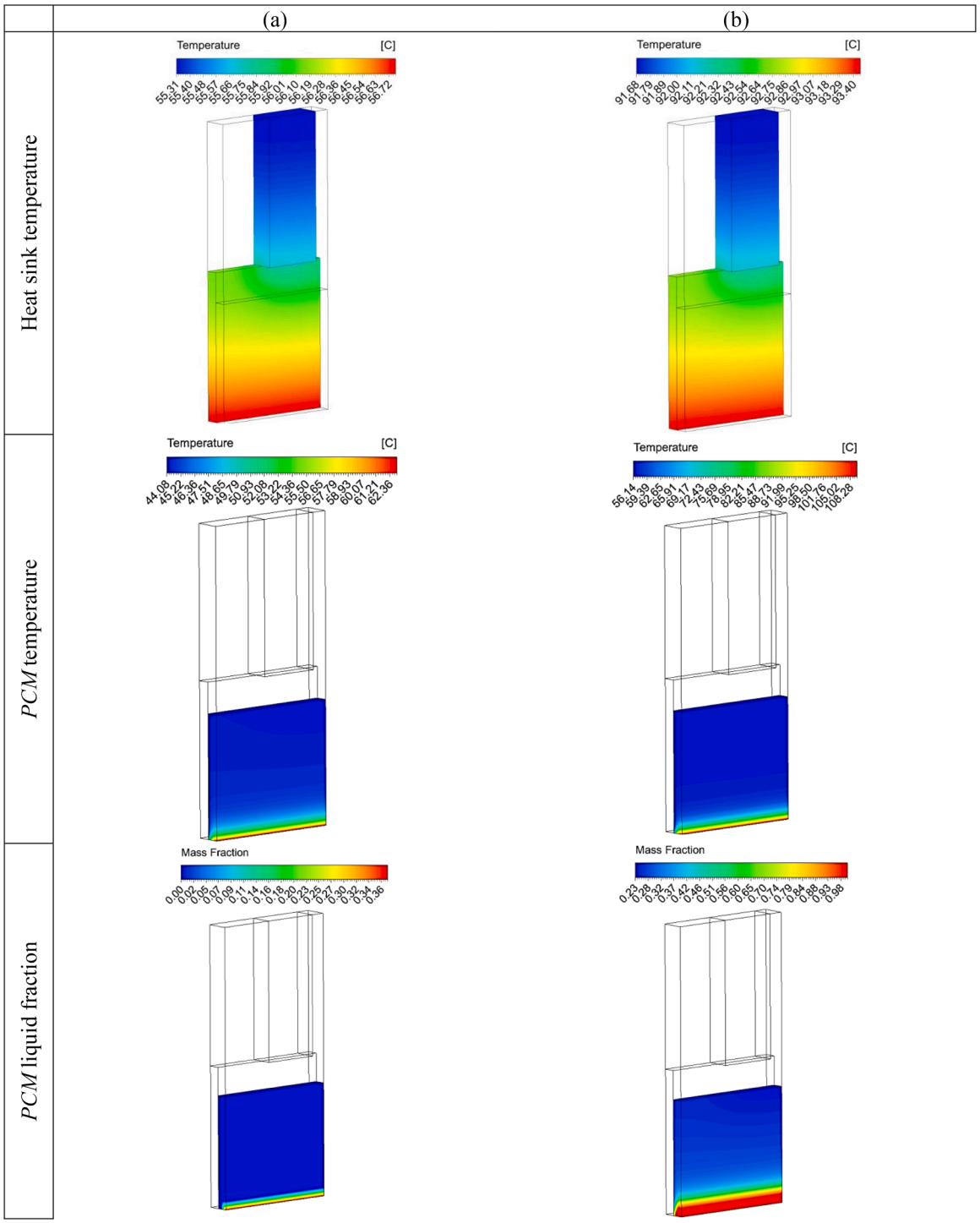

Fig. 12. Temperature of the heat sink, *PCM* and liquid fraction at heat fluxes of a) 160 and b) 190kW/m^2 in natural convection mode.

for lower heat flux. This fact which is the result of a lower temperature gradient at low heat fluxes shows that at low heat fluxes, increasing the *Re* number does not work well and does not decrease heat sink temperature effectively. In fact, at the highest heat flux values, the *Re* number elevation has the most effect on the heat transfer coefficient. The *Nu* number against the *Re* number in the case of $\ddot{q} = 150\frac{kW}{m^2}$ is depicted in Fig. 6. As seen, by growing the *Re* number from 20 to 60, the *Nu* number increased by 24 %.

The pressure drop and *Nu* number grow simultaneously with the *Re* number increase. The pressure drop variation against the *Re* number is illustrated in Fig. 7; it is revealed that the pressure drop growth resulting from the *Re* number increase from 20 to 60 is nearly 430 %; this figure should be compared to a 24 % improvement of *Nu* number due to *Re* number increment which warns about selecting the proper *Re* number. It would be more beneficial to possibly get away with using the high *Re* numbers.

To better visualize the heat sink from its thermal performance viewpoint, the temperature contours in both solid and air sides and different *Re* numbers are illustrated in Fig. 8; it could be inferred that increasing the *Re* number, reduces the zone of high temperature in the solid side; the mean temperature of heat sink is199, 126 and 92.5 °C at *Re* numbers of 20, 40 and 60 which shows vividly the influence of *Re*

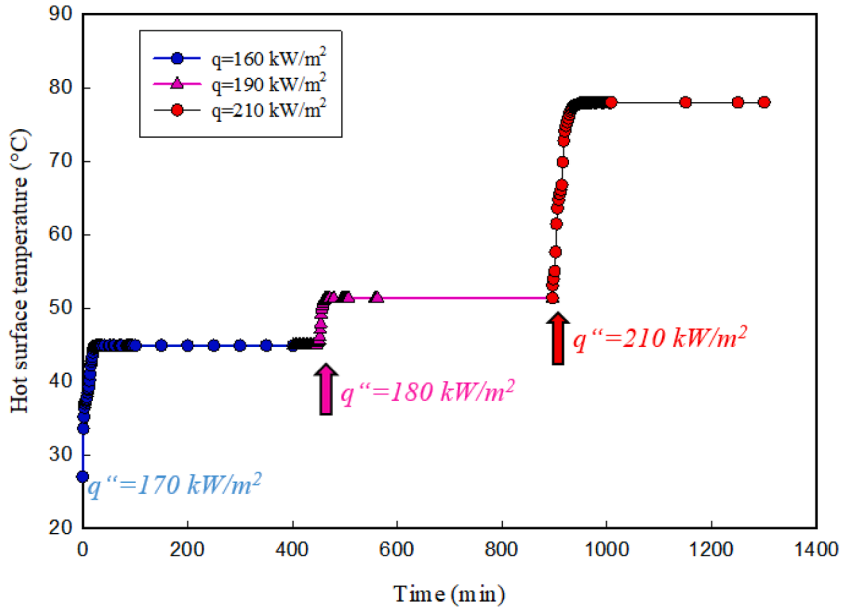

Fig. 13. The time variation of *PCM* embedded heat sink temperature at *Re* = 20 during the heat absorption.

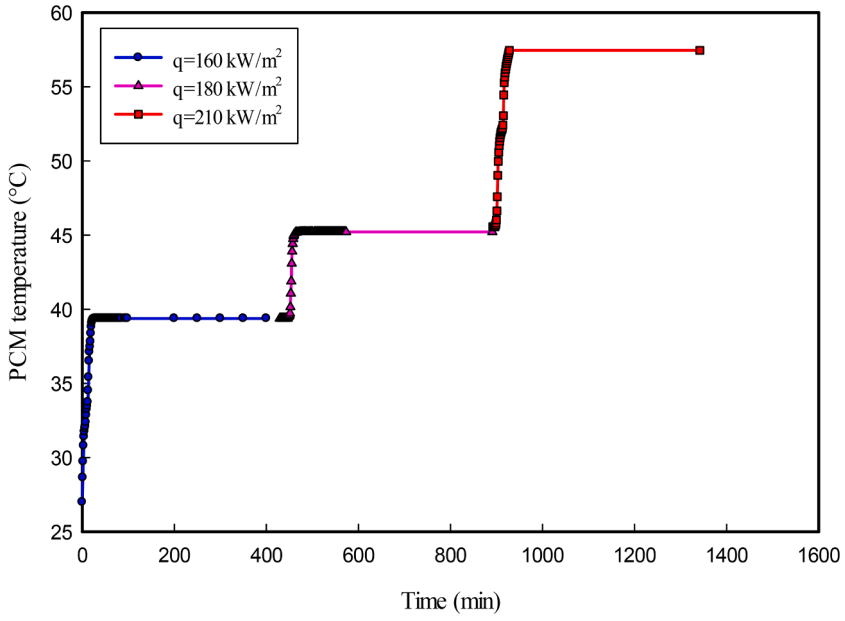

Fig. 14. The *PCM* average temperature changes vs the time at *Re*=20 during heat absorption.

number increase on cooling. Moreover, on the air side, by the *Re* number enlargement, the temperature gradient becomes smaller which results in an overall more uniform temperature field; the temperature change through the air pathway is 167, 96 and 64 °C at *Re* numbers of 20, 40 and 60. In the case of *Re* = 40 and 60, the temperature gradient in the horizontal path of airflow is higher which shows an enhanced heat exchange.

To understand further the effect of airflow and *Re* number on the rate of heat transfer the air streamlines for different *Re* numbers are illustrated in Fig. 9. As shown, by elevating the *Re* number the point of separation goes toward the inlet and the heat transfer enhancing effect of wakes gets more pronounced throughout the air path. This, as was seen before, would result in a more uniform temperature distribution and a smaller temperature gradient inside the air path would be generated.

4.2. Heat sink with the embedded PCM

4.2.1. Natural convection mode

By its latent heat of phase change, the *PCM* embedded inside the heat sink would absorb the heat and prevent overheating. It is mainly the phase change temperature of *PCM* which governs the heat sink temperature. Therefore the enhancing effect of *PCM* addition on thermal management of heat sinks could be predicted. Considering the unsteady nature of phase change (melting and solidification), the system performance is described vs the time. The *PCM* temperature during the heat absorption is illustrated in Fig. 10. As seen, by applying the *HF* and increasing it at four stages of 150, 170, 180 and 190 kW/m^2, the *PCM* temperature increased gradually and reached 40, 45, 53 and 59 °C, respectively. Remarkably, the presence of *PCM* increases the thermal mass of the system and hence its response time. Considering the large

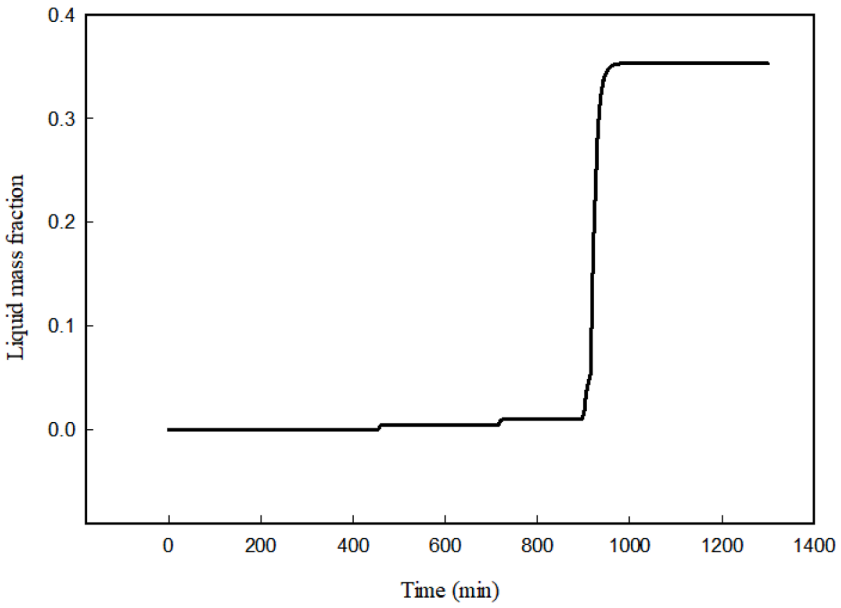

Fig. 15. The *PCM* liquid fraction change vs time during the heat flux input.

period of applying heat flux (200 min at each time step) the system has enough time to change its situation without exceeding the allowable temperature. To be more elucidated the heat sink temperature vs the time is seen in Fig. 11.

The heat sink temperature in Fig. 11 shows a stepwise change that is similar to *PCM* temperature change; the average temperature of the heat sink is 44, 52, 72 and 75 °C for heat fluxes of 150, 170, 180 and 190kW/m^2, respectively. These temperatures should be compared to a temperature of 145 °C which was the plate's average temperature in case of using no *PCM* (Section 4.1); as seen, embedding the *PCM* in the heat sink reduces its temperature significantly. The observed delay time of temperature increase is the result of phase change latent heat which keeps and controls the plate temperature within the allowable limit during the working time. The contours of the *PCM* and heat sink temperature and *PCM* liquid fraction at heat fluxes are depicted in Fig. 12.

By inspecting the contours of the heat sink and *PCM* temperature, it could be seen that by its capacity of latent heat storage, the *PCM* alleviates the temperature growth. This effect could be seen in *PCM* liquid fraction contours; the liquid phase in the vicinity of input heat flux propagates outward and absorbs the heat. Also, the zone of the liquid phase has been increased at elevated heat flux input. The relatively small part of the liquid phase near the hot surface is attributed to the low thermal conductivity of the *PCM*.

4.2.2. Forced convection mode

It was seen previously that the forced convection mode has priority in cooling the *MCHSs*. Besides the beneficial feature, the dependency of forced convection mode on using the external power for the air circulator, the application of forced convection is rational well at the lowest *Re* number. The time variation of *PCM* embedded heat sink temperature at *Re* number of 20 is seen in Fig. 13; the heat sink temperature at heat fluxes of 150, 190 and 210kW/m^2 are 45, 52 and 78 °C, respectively. The heat sink temperature is 44, 52, 72 and 75 °C for heat fluxes of 150, 170, 190 and 210 kW/m^2, respectively. It could be compared to a similar case without the embedded *PCM* which resulted in a heat sink temperature of 200 °C at a heat flux of 150kW/m^2. This high value of temperature reduction (75 than 200 °C) is due to *PCM* melting near the hot surface whose temperature distribution vs. the time is in Fig. 14.

The stepwise increment of *PCM* average temperature vs the time shows the growth of molten front by the time; regarding the *PCM* melting point temperature of 58 °C, at the second stage, by the mean *PCM* temperature of 47 °C, the major part of *PCM* is still solid. By the heat flux increment to 120kW/$m^{2,}$ the mean temperature reaches to vicinity of the melting point which elevates the average *PCM* temperature to 51 °C. The change in the *PCM* liquid fraction is depicted in Fig. 16.

By inspecting the *PCM* liquid fraction in Fig. 15 it could be revealed that the heat flux below 210kW/m^2 is not enough to melt the *PCM* considerably; 1000 min is the time that the *PCM* begins to melt and the growth of the melting front causes the increment of its average temperature (Fig. 14); this also could be inferred from the *PCM* and heat sink temperature contours and the *PCM* liquid fraction (Fig. 16). The heat flux of 160kW/m^2 cannot generate a complete liquid phase and a mixture of 65 % - 35 % solid-liquid phase is observed near the hot wall. Instead by increasing the heat flux to 210 kW/m^2, a liquid phase with a temperature of 115 °C is generated near the wall. By generating a relatively big melted front, the existence of the *PCM* module with its large *LTES* keeps the heat sink temperature below 57 °C

5. Conclusion

The development of industries relies heavily on developing electronic systems. The need for miniaturization electronic circuits (*ECs*) and the resulting problem of overheating, make the thermal management of these systems an inevitable task. By its high surface-to-volume ratio, the microchannel heat sink (*MCHS*) performance is considered a successful solution for cooling compact thermal systems. In addition, by the potential of latent thermal storage, the effect of using phase change material (*PCM*) on cooling the *MCHS* was investigated. The heat transfer modes of free and forced convection in systems with and without the *PCM* were studied. The employed *PCM* is paraffin wax and the system performance was analyzed under five input heat fluxes and three *Re* numbers. The obtained results could be summarized as follows.

- The results demonstrated the outstanding effect of the *PCM* employment on controlling the temperature of *EC*; in natural convection mode embedding the *PCM* board reduces the heat sink temperature by 72 % (from 145 to 40 °C) and makes the possible working of *EC* without overheating.
- The airflow and switching the heat transfer from natural to forced convection has a beneficial effect on cooling the board even when no *PCM* was employed. Furthermore, the *Re* number increase has the

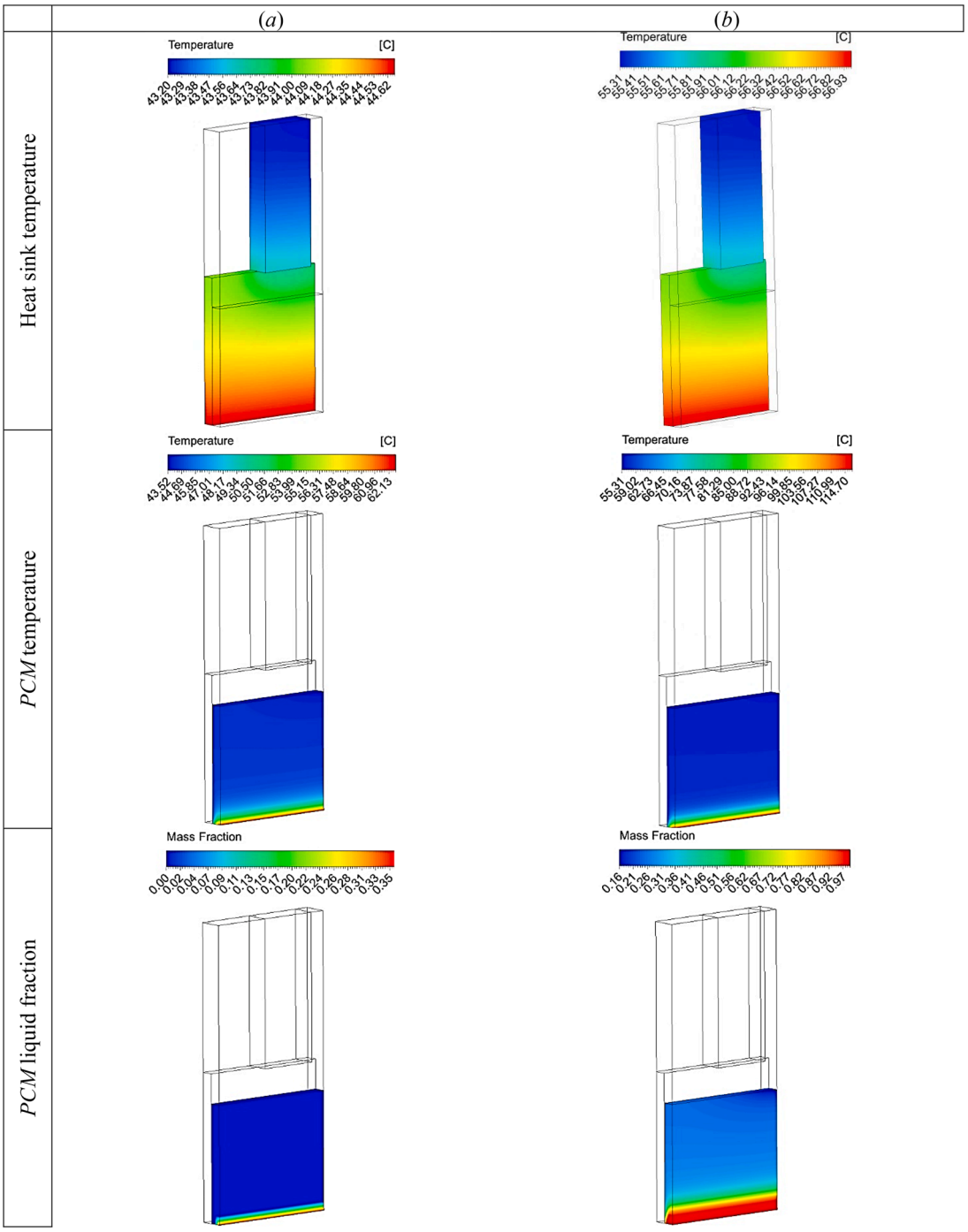

Fig. 16. Heat sink temperature, *PCM* temperature and liquid fraction at heat fluxes of *a*) 160 and *b*) 190kW/m^2 in forced convection mode.

best effect on cooling efficiency at higher heat fluxes. By elevating the *Re* from 20 to 60, the mean temperature reduced by 50 %, 40 % and 11 % at heat fluxes of 150, 80 and 40 kW/m^2, respectively.

- Although applying the airflow and switching from natural convection to forced one has a decreasing effect on *EC* temperature, the application of the *PCM* board attenuates the mean temperature more; in forced convection mode with $Re = 20$, the insertion of *PCM* reduces the plate mean temperature by 78 % (from 200 to 45 °C).
- The findings of the present work confirm the application of *PCM* in *MCHS* technically and could be used in justifying the economical features in designing heat dissipation systems.

CRediT authorship contribution statement

Ali B.M. Ali: Conceptualization, Data curation, Formal analysis, Funding acquisition, Investigation, Methodology, Project administration, Resources, Software, Supervision, Validation, Visualization, Writing – original draft, Writing – review & editing. **Sabah F.H. Alhamdi:** Conceptualization, Data curation, Formal analysis, Funding acquisition, Investigation, Methodology, Project administration, Resources, Software, Supervision, Validation, Visualization, Writing – original draft, Writing – review & editing. **Mohammad M.S. Al-Azawii:** Conceptualization, Data curation, Formal analysis, Funding acquisition, Investigation, Methodology, Project administration, Resources, Software, Supervision, Validation, Visualization, Writing – original draft,

Writing – review & editing. **Narinderjit Singh Sawaran Singh:** Conceptualization, Data curation, Formal analysis, Funding acquisition, Investigation, Methodology, Project administration, Resources, Software, Supervision, Validation, Visualization, Writing – original draft, Writing – review & editing. **Mohammad Ali Fazilati:** Conceptualization, Data curation, Formal analysis, Funding acquisition, Investigation, Methodology, Project administration, Resources, Software, Supervision, Validation, Visualization, Writing – original draft, Writing – review & editing. **Soheil Salahshour:** Conceptualization, Data curation, Formal analysis, Funding acquisition, Investigation, Methodology, Project administration, Resources, Software, Supervision, Validation, Visualization, Writing – original draft, Writing – review & editing. **S. Ali Eftekhari:** Conceptualization, Data curation, Formal analysis, Funding acquisition, Investigation, Methodology, Project administration, Resources, Software, Supervision, Validation, Visualization, Writing – original draft, Writing – review & editing.

Declaration of competing interest

The authors declare that they have no known competing financial interests or personal relationships that could have appeared to influence the work reported in this paper.

Data availability

No data was used for the research described in the article.

References

[1] Y. Lan, Z. Feng, K. Huang, J. Zhang, Z. Hu, Effects of truncated and offset pin-fins on hydrothermal performance and entropy generation in a rectangular microchannel heat sink with variable fluid properties, Int. Commun. Heat Mass Transf. 124 (2021) 105258.

[2] C. Ho, Y.-C. Liu, M. Ghalambaz, W.-M. Yan, Forced convection heat transfer of Nano-encapsulated phase change material (NEPCM) suspension in a mini-channel heatsink, Int. J. Heat Mass Transf. 155 (2020) 119858.

[3] Y. Ma, A. Shahsavar, P. Talebizadehsardari, Two-phase mixture simulation of the effect of fin arrangement on first and second law performance of a bifurcation microchannels heatsink operated with biologically prepared water-Ag nanofluid, Int. Commun. Heat Mass Transf. 114 (2020) 104554.

[4] Z. Li, H. Luo, Y. Jiang, H. Liu, L. Xu, K. Cao, H. Wu, P. Gao, H. Liu, Comprehensive review and future prospects on chip-scale thermal management: core of data center's thermal management, Appl. Therm. Eng. (2024) 123612.

[5] P. Bhandari, K.S. Rawat, Y.K. Prajapati, D. Padalia, L. Ranakoti, T. Singh, A review on design alteration in microchannel heat sink for augmented thermohydraulic performance, Ain Shams Eng. J. 15 (2024) 102417.

[6] D.B. Tuckerman, R.F.W. Pease, High-performance heat sinking for VLSI, IEEE Electron Dev. Lett. 2 (1981) 126–129.

[7] R.A. Saini, M. Vohra, A. Singh, T. Rabbani, M. Choudhary, Comparative thermal performance evaluation of a heat sink based on geometrical and material amendments: a numerical study, Mater. Today: Proceed. 50 (2022) 816–822.

[8] Ö. Bayer, S.B. Oskouei, S. Aradag, Investigation of double-layered wavy microchannel heatsinks utilizing porous ribs with artificial neural networks, Int. Commun. Heat Mass Transf. 134 (2022) 105984.

[9] H.A. Kose, A. Yildizeli, S. Cadirci, Parametric study and optimization of microchannel heat sinks with various shapes, Appl. Therm. Eng. 211 (2022) 118368.

[10] M. Gorzin, A. Ranjbar, M. Hosseini, Experimental and numerical investigation on thermal and hydraulic performance of novel serpentine minichannel heat sink for liquid CPU cooling, Energy Rep. 8 (2022) 3375–3385.

[11] V. Gaikwad, S. Mohite, Performance analysis of microchannel heat sink with flow disrupting pins, J. Therm. Eng. 8 (2022) 402–425.

[12] R. Shailendra, H.B. DURA, S. BHATTRAI, R. SHRESTHA, Impact of baffle on forced convection heat transfer of CuO/water nanofluid in a micro-scale backward facing step channel, J. Therm. Eng. 8 (2022) 310–322.

[13] A.M. Sahar, J. Wissink, M.M. Mahmoud, T.G. Karayiannis, M.S.A. Ishak, Effect of hydraulic diameter and aspect ratio on single phase flow and heat transfer in a rectangular microchannel, Appl. Therm. Eng. 115 (2017) 793–814.

[14] S. Bazkhane, I. Zahmatkesh, Taguchi–based sensitivity analysis of hydrodynamics and heat transfer of nanofluids in a microchannel heat sink (MCHS) having porous substrates, Int. Commun. Heat Mass Transf. 118 (2020) 104885.

[15] N.R. Kuppusamy, H.A. Mohammed, C.W. Lim, Thermal and hydraulic characteristics of nanofluid in a triangular grooved microchannel heat sink (TGMCHS, Appl. Math. Comput. 246 (2014) 168–183.

[16] N.R. Kuppusamy, H. Mohammed, C.W. Lim, Numerical investigation of trapezoidal grooved microchannel heat sink using nanofluids, Thermochim. Acta 573 (2013) 39–56.

[17] H. Dai, W. Chen, Numerical investigation of heat transfer in the double-layered minichannel with microencapsulated phase change suspension, Int. Commun. Heat Mass Transf. 119 (2020) 104918.

[18] M. Kumar, V. Bisht, S.S. Chandel, S. Sinha-Ray, P. Kumar, Convective flow of nanofluid and nanoencapsulated phase change material through microchannel heat sink for passive cooling of microelectronics, in: Proc. Recent Advances in Mechanical Engineering: Select Proceedings of ICRAME 2020, Springer, 2021, pp. 51–60.

[19] V. Kumar, J. Sarkar, Experimental hydrothermal behavior of hybrid nanofluid for various particle ratios and comparison with other fluids in minichannel heat sink, Int. Commun. Heat Mass Transf. 110 (2020) 104397.

[20] R. Chein, G. Huang, Analysis of microchannel heat sink performance using nanofluids, Appl. Therm. Eng. 25 (2005) 3104–3114.

[21] S. Motahar, M. Jahangiri, Transient heat transfer analysis of a phase change material heat sink using experimental data and artificial neural network, Appl. Therm. Eng. 167 (2020) 114817.

[22] M.A. Fazilati, A.A. Alemrajabi, Phase change material for enhancing solar water heater, an experimental approach, Energy Convers. Manage. 71 (2013) 138–145.

[23] F. Li, A.M. Abed, O. Naghdi, N. Nasajpour-Esfahani, S. Hamedi, Z.I. Al Mashhadani, M.A. Fazilati, B.M. Mohammed, S.K. Hadrawi, G.F. Smaisim, The numerical investigation of the finned double-pipe phase change material heat storage system equipped with internal vortex generator, J. Energy Storage 55 (2022) 105413.

[24] A. Mourad, A. Aissa, A.M. Abed, G.F. Smaisim, D. Toghraie, M.A. Fazilati, O. Younis, K. Guedri, A.A. Alizadeh, The numerical analysis of the melting process in a modified shell-and-tube phase change material heat storage system, J. Energy Storage 55 (2022) 105827.

[25] H. Faraji, A. Benkaddour, K. Oudaoui, M. El Alami, M. Faraji, Emerging applications of phase change materials: a concise review of recent advances, Heat Transf. 50 (2021) 1443–1493.

[26] H. Saleh, Z. Siri, M. Ghalambaz, Natural convection from a bottom heated of an asymmetrical U-shaped enclosure with nano-encapsulated phase change material, J. Energy Storage 38 (2021) 102538.

[27] S.-R. Yan, M.A. Fazilati, N. Samani, H.R. Ghasemi, D. Toghraie, Q. Nguyen, A. Karimipour, Energy efficiency optimization of the waste heat recovery system with embedded phase change materials in greenhouses: a thermo-economic-environmental study, J. Energy Storage 30 (2020) 101445.

[28] V. Bianco, M. De Rosa, K. Vafai, Phase-change materials for thermal management of electronic devices, Appl. Therm. Eng. 214 (2022) 118839.

[29] M.G. Izenson, D.A. Knaus, L. O'Neill, Thermal Storage for High-Power Small Satellites, 2020. Vol.

[30] W. Hua, L. Zhang, X. Zhang, Research on passive cooling of electronic chips based on PCM: a review, J. Mol. Liq. 340 (2021) 117183.

[31] A.R. Dhumal, A.P. Kulkarni, N.H. Ambhore, A comprehensive review on thermal management of electronic devices, J. Eng. Appl. Sci. 70 (2023) 140.

[32] H.M. Maghrabie, K. Elsaid, T. Wilberforce, E.T. Sayed, M.A. Abdelkareem, A. G. Olabi, Applications of nanofluids in cooling of electronic components. Encyclopedia of Smart Materials, Elsevier, 2021, pp. 310–318.

[33] P. Rosa, T. Karayiannis, M. Collins, Single-phase heat transfer in microchannels: the importance of scaling effects, Appl. Therm. Eng. 29 (2009) 3447–3468.

[34] D. Zhou, C.-Y. Zhao, Y. Tian, Review on thermal energy storage with phase change materials (PCMs) in building applications, Appl. Energy 92 (2012) 593–605.

[35] P.J. Shamberger, Cooling capacity figure of merit for phase change materials, J. Heat Transf. 138 (2016) 024502.

[36] W.-M. Yan, C. Ho, Y.-T. Tseng, C. Qin, S. Rashidi, Numerical study on convective heat transfer of nanofluid in a minichannel heat sink with micro-encapsulated PCM-cooled ceiling, Int. J. Heat Mass Transf. 153 (2020) 119589.

[37] Y. Wang, D.J. Jasim, S. Mohammad Sajadi, G. Fadhil Smaisim, S.K. Hadrawi, N. Nasajpour-Esfahani, M. Alizade, M. Zarringhalam, S. Salahshour, D. Toghraie, Experimental study of phase change material (PCM) based spiral heat sink for the cooling process of electronic equipment, Ain Shams Eng. J. 15 (2024) 102793.

[38] M.I. Hasan, H.L. Tbena, Using of phase change materials to enhance the thermal performance of micro channel heat sink, Eng. Sci. Technol., Int. J. 21 (2018) 517–526.

[39] Y. Chen, Y. Zhuang, J.-C. Feng, S.-M. Huang, Numerical investigation on flow and heat transfer characteristics in honeycomb-like microchannel heat sink encapsulated with phase change material, Appl. Therm. Eng. 232 (2023) 121060.

[40] N.R. Korasikha, T. Karthikeya Sharma, G. Amba Prasad Rao, Numerical investigation on hydrothermal characteristics of microchannel heat sinks with PCM inserts for effective thermal management applications, Int. J. Num. Method. Heat Fluid Flow 35 (2025) 140–167.

[41] E. Kyriaki, C. Konstantinidou, E. Giama, A.M. Papadopoulos, Life cycle analysis (LCA) and life cycle cost analysis (LCCA) of phase change materials (PCM) for thermal applications: a review, Int. J. Energy Res. 42 (2018) 3068–3077.

[42] M. Hosseini, A. Ranjbar, K. Sedighi, M. Rahimi, A combined experimental and computational study on the melting behavior of a medium temperature phase change storage material inside shell and tube heat exchanger, Int. Commun. Heat Mass Transf. 39 (2012) 1416–1424.

[43] S.V. Patankar, Numerical Heat Transfer and Fluid Flow(Book), Hemisphere Publishing Corp., Washington, DC, 1980, p. 210, 1980.

[44] M. Hosseini, M. Rahimi, R. Bahrampoury, Experimental and computational evolution of a shell and tube heat exchanger as a PCM thermal storage system, Int. Commun. Heat Mass Transf. 50 (2014) 128–136.

[45] P. Barnoon, D. Toghraie, B. Mehmandoust, M.A. Fazilati, S.A. Eftekhari, Comprehensive study on hydrogen production via propane steam reforming inside a reactor, Energy Rep. 7 (2021) 929–941.
[46] S. Hosseinizadeh, F. Tan, S. Moosania, Experimental and numerical studies on performance of PCM-based heat sink with different configurations of internal fins, Appl. Therm. Eng. 31 (2011) 3827–3838.
[47] M.H. Esfe, H. Mazaheri, S.S. Mirzaei, E. Kashi, M. Kazemi, M. Afrand, Effects of twisted tapes on thermal performance of tri-lobed tube: an applicable numerical study, Appl. Therm. Eng. 144 (2018) 512–521.